

Chemical Bonding Nature and Mesoporous Structure of Nickel Intercalated Montmorillonite Clay

Hye Mi Park, Tae Woo Kim, Seong-Ju Hwang,* and Jin-Ho Choy*

Center for Intelligent Nano-Bio Materials (CINBM), Division of Nano Sciences and Department of Chemistry, Ewha Womans University, Seoul 120-750, Korea. *E-mail: hwangsju@ewha.ac.kr

Received May 24, 2006

Mesoporous nickel intercalated aluminosilicate nanohybrid has been synthesized through a recombination reaction between the colloidal suspension of exfoliated montmorillonite nanosheets and aqueous nickel acetate solution. According to powder X-ray diffraction and field emission-scanning electron microscopic analyses, the intercalation of nickel species expands significantly the basal spacing of the host montmorillonite clay and the crystallites of the intercalation compound are assembled to form a house-of-card structure. N₂ adsorption-desorption isotherm measurements with BJH pore analyses clearly demonstrated that the porosity of the intercalate originates mainly from mesopores (diameter ~50 Å) formed by the house-of-card type stacking of clay crystallites. From FT-IR and X-ray absorption spectroscopic analyses, it becomes certain that intercalated nickel ion is stabilized in an isolated NiO₆ octahedral unit. The present mesoporous intercalation compound is expected to be applicable as efficient catalysts or absorbents.

Key Words : Ni-intercalated montmorillonite clay, Nanohybrid, Mesoporosity, Exfoliation-restacking, House-of-card structure

Introduction

Over the past decades, extensive research activities have been devoted for the intercalation compounds of aluminosilicate clay minerals since the incorporation of inorganic pillars into the 2D clay lattice gives rise to a significant increase of surface area through the formation of micropores in the interlayer space.¹⁻³ In particular, the intercalation of transition metal compound into the clay can provide an opportunity to develop excellent heterogeneous catalysts with an expanded surface area. As a consequence, transition metal oxide-intercalated clay systems such as CoO/SiO₂,⁴ Cr₂O₃,⁵ Fe₂O₃,⁶ ZrO₂,⁷ TiO₂,⁸ ZnO-aluminosilicate⁹ have been reported. In most cases, such intercalation compounds were synthesized through an ion-exchange reaction between interlayer alkali metal cation in the clay and the positively charged guest species. Among transition metal elements, nickel metal and its compounds have been widely used as redox catalysts for various chemical reactions and anodic electrodes for electrochromic devices and rechargeable batteries.¹⁰⁻¹² Such an activity of these compounds can be enhanced through the formation of porous intercalation complex. However, a porous intercalative nanohybrid of the aluminosilicate clay with nickel species has less been investigated. Instead, there have several studies on nonporous heterostructured materials consisting of alternating 2D nickel hydroxide layers and the host clay layers.^{13,14} This compound was synthesized by the intercalation of nickel ions into the clay lattice and the subsequent hydroxylation of intercalated nickel ions, leading to the formation of CdI₂-type nickel hydroxide network in-between the clay lattice.¹³ Alternatively, an indirect synthesis of nickel-containing porous compound was achieved by the incorporation of

nickel hydroxide into the micropores of alumina-pillared clays.¹⁵ However, due to the limitation of lattice expansion, it is difficult to prepare mesoporous materials through the pillaring of clay mineral. Recently it was reported that mesoporous clay-based aluminosilicates could be obtained *via* an exfoliation-restacking reaction,¹⁶ in which the 2D lattice of aluminosilicate clay was separated into individual monolayers and then the exfoliated clay nanosheets with negative surface charge combine with positively charged transition metal species. Under this synthetic condition, the crystallites of the intercalation compound easily form the house-of-card type structure containing high concentration of mesopores.

In this study, we were successful in synthesizing mesoporous nickel-incorporated montmorillonite *via* the exfoliation-restacking method. The crystal structure, chemical composition, and pore structure of the obtained intercalate have been systematically characterized using powder X-ray diffraction (XRD), X-ray fluorescence spectroscopy (XRF), thermogravimetric analysis (TGA), diffuse reflectance UV-vis spectroscopy, field emission-scanning electron microscopy (FE-SEM), and N₂ adsorption-desorption isotherm measurement. Also, Fourier transformed-infrared (FT-IR) and X-ray absorption spectroscopic (XAS) analyses have been performed to probe the chemical bonding nature of the intercalated nickel species.

Experimental Section

Pristine montmorillonite clay (Kunipia Co.) was treated with excess 1 M NaCl aqueous solution for several times and then dried at 50 °C. The obtained powder was dispersed in a distilled water for 1 week to prepare the colloidal

suspension of delaminated clay particles.⁹ The nickel intercalated montmorillonite was synthesized by reacting the colloidal suspension of the montmorillonite clay with the aqueous solution of nickel acetate at 80 °C for 3 days under reflux condition. Prior to characterization, the product was washed thoroughly with distilled water and then dried. The crystal structure, crystallite morphology, and optical property of the nickel intercalated montmorillonite were studied by powder XRD, FE-SEM (JEOL JSM-6700F microscope), and diffuse reflectance UV-vis spectroscopy (Perkin-Elmer lambda 35 spectrometer), respectively. Their chemical composition, thermal behavior, lattice vibration, and surface area/porosity were determined by XRF, TGA, FT-IR, and N₂ adsorption-desorption isotherm measurements, respectively. XAS experiments were carried out at the Ni K-edge with the extended X-ray absorption fine structure (EXAFS) facility installed at the beam line 7C at the Pohang Light Sources (PLS) in Korea. XAS data were collected at room temperature in a transmission mode using gas-ionization detectors. All the present spectra were calibrated carefully by measuring the reference spectrum of Ni metal simultaneously. Data analysis for the experimental spectra was performed with a standard procedure, as reported previously.¹⁷ In the course of EXAFS fitting analysis on the reference Ni(OH)₂, the coordination number (*CN*) was fixed to the crystallographic values, whereas the amplitude reduction factor (*S₀²*) was allowed to vary. As for the intercalates, the *CN* of (Ni-O) shell was set as variables to determine the local geometry of the intercalated nickel ions with reference to the *S₀²* factor calculated from the reference Ni(OH)₂. All the bond distances (*R*), energy shifts (ΔE), and Debye-Waller factors (σ^2) were set as variables.

Results and Discussion

The powder XRD patterns of nickel-intercalated montmorillonite and its calcined derivative are presented in Figure 1, in comparison with that of the pristine Na-montmorillonite. Upon the intercalation of nickel species, (*00l*) reflections move toward low angle side, indicating the increase of basal spacing. From the least square fitting analysis, the basal spacing of the as-prepared intercalate was determined to be 14.6 Å, corresponding to the gallery height of 5.0 Å. A similar degree of lattice expansion was reported for the interstratified compound consisting of alternating metal hydroxide layers and the host aluminosilicate ones.¹³ While the previously reported interstratified compound with 2D nickel hydroxide layers shows more intense (*00l*) reflections with *l* > 2 than (*001*) reflection, the present Ni-intercalation compound displays the strongest intensity for the (*001*) reflection. Such a dissimilar distribution in the intensities of (*00l*) reflections reflects the increase of structural disorder due to the weakening of interlayer interaction of the host layers upon the intercalation of isolated nickel species. As shown in Figure 1, a heat-treatment at 200 °C makes the expanded structure of the Ni-intercalate collapsed to the basal spacing of 12.5 Å. Such a weak thermal stability

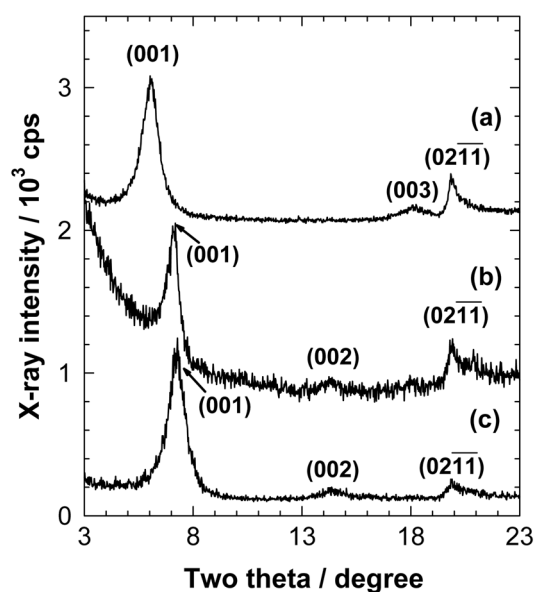


Figure 1. Powder XRD patterns of (a) the nickel-intercalated montmorillonite and (b) its derivative calcined at 200 °C, in comparison with that of (c) the pristine Na-montmorillonite.

of the present intercalate is surely due to the absence of highly linked 2D network of nickel hydroxide species. In fact, the previously reported interstratified compound with intercalated 2D metal hydroxide layer shows much better thermal stability than the present compound.¹³

According to XRF analysis, it was found that considerable amount of nickel species are intercalated into the clay lattice with the Ni/Al ratio of 0.24. With reference to the chemical composition of host compound, the chemical composition of the resulting intercalate was determined to be Ni_{0.42}(Na_{0.35}-K_{0.01}Ca_{0.02})(Si_{3.89}Al_{0.11})-(Al_{1.60}Fe_{0.08}Mg_{0.32})O₁₀(OH)₂·2.37H₂O. Also, the thermal behavior of the present intercalate was examined by performing TGA measurement under Ar

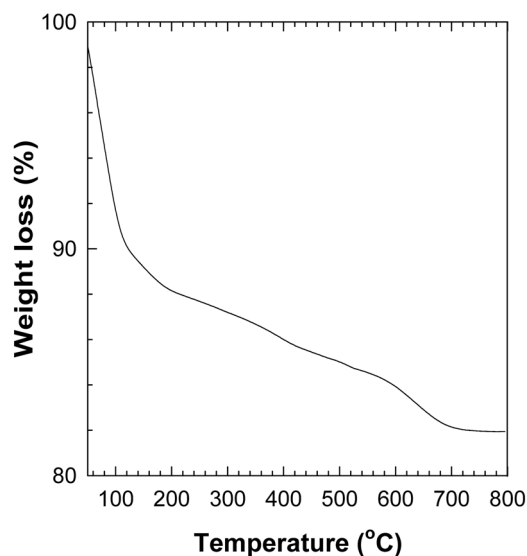


Figure 2. TGA curve of the nickel-intercalated montmorillonite under Ar atmosphere.

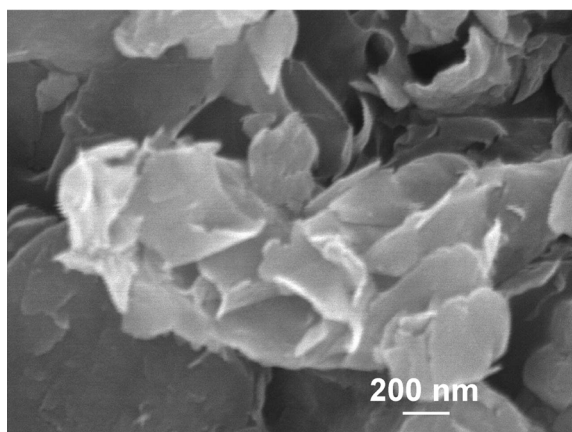


Figure 3. FE-SEM image of the nickel-intercalated montmorillonite.

atmosphere. As shown in Figure 2, there occur three steps of weight loss in the present TGA curve of the nickel-intercalated montmorillonite. While the first weight decrease in the temperature range of 50-250 °C is attributable to the evaporation of water molecules in the sample, the dehydroxylation of the host lattice would be responsible for the second weight loss in the temperature range of 250-600 °C. From a weight decrease at the first step, the water content was determined to be 5.6 molecules per each nickel ion. The third weight loss beyond 600 °C possibly occurs due to an evaporation of interlayer sodium cations.

We have examined the crystallite morphologies of the nickel-intercalated montmorillonite using FE-SEM. As shown in Figure 3, the layered crystallites of montmorillonite with the lateral dimension of 400-500 nm are restacked to form a house-of-card structure.

Figure 4 illustrates the N₂ adsorption-desorption isotherms of the as-prepared nickel-intercalated montmorillonite and its calcined derivative at 200 °C. A distinct hysteresis is

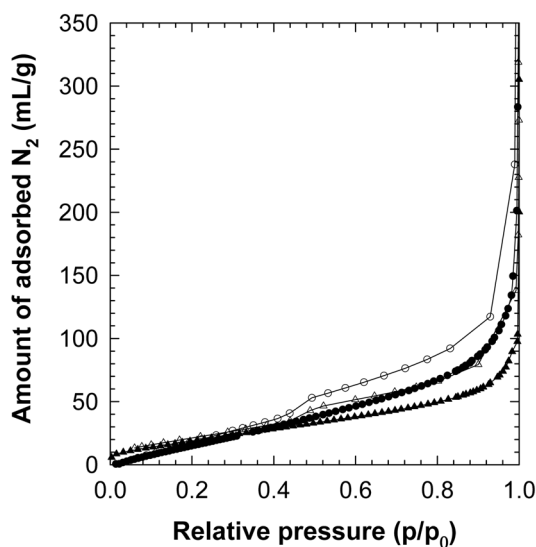


Figure 4. N₂ adsorption-desorption isotherms for the nickel-intercalated montmorillonite (circles) and its derivative calcined at 200 °C (triangles).

detectable in the pressure region of $p/p_0 > 0.5$ for both the present samples, indicating the formation of mesoporous structure originating from the house-of-card stacking of the crystallites. The present isotherm data can be classified as the BDDT type I and IV shape, along with H4-type hysteresis loop in the IUPAC classification.¹⁸ Such a type of isotherm underlines the presence of the open slit-shaped capillaries with very wide bodies and narrow short necks. In comparison with the mesopores, the micropores originated from the intercalation structure make only a smaller contribution to total surface area. This is due to the fact that the presence of interlayer water molecules occupying the micropores would prevent the efficient introduction and adsorption of nitrogen molecules into the gallery space of the intercalate. After the calcination at 200 °C, the nitrogen adsorption in a low p/p_0 region becomes slightly increased, which is due to the opening of micropores by the removal of water from the interlayer space. In comparison with the pristine montmorillonite with the surface area of $\sim 25 \text{ m}^2 \text{ g}^{-1}$, the intercalates have much greater surface area of $\sim 240 \text{ m}^2 \text{ g}^{-1}$ for the as-prepared sample and $\sim 78 \text{ m}^2 \text{ g}^{-1}$ for the calcined derivative. The pore distribution of the intercalates was analyzed by performing pore size analysis with BJH method. As shown in Figure 5, the pore-size analysis demonstrates that the as-prepared intercalate and its calcined derivative have a similar pore distribution with an average pore diameter of $\sim 5 \text{ nm}$. Although the calcination depresses the basal spacing of the intercalate to that of the pristine materials (Fig. 1), the surface area and mesoporosity of the calcined derivative are still maintained to be much greater than those of the pristine clay mineral. This finding suggests that, even after the calcination, this mesoporous intercalation compound would be applicable as efficient catalysts or absorbents.

Diffuse reflectance UV-vis spectrum for the nickel-intercalated montmorillonite is illustrated in Figure 6, together

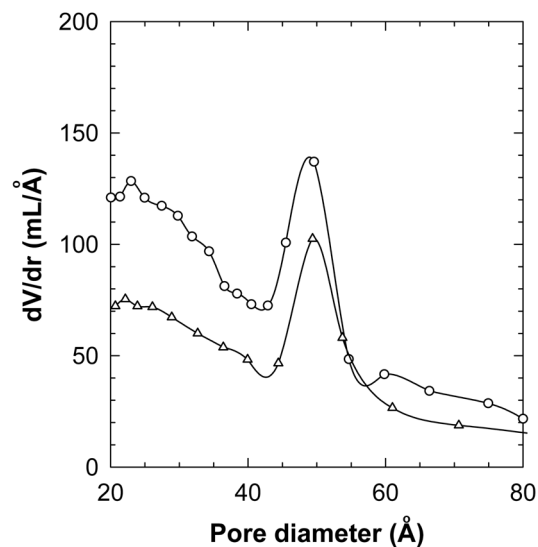


Figure 5. Pore size distribution curve for the nickel-intercalated montmorillonite (circles) and its derivative calcined at 200 °C (triangles) analyzed by BJH method.

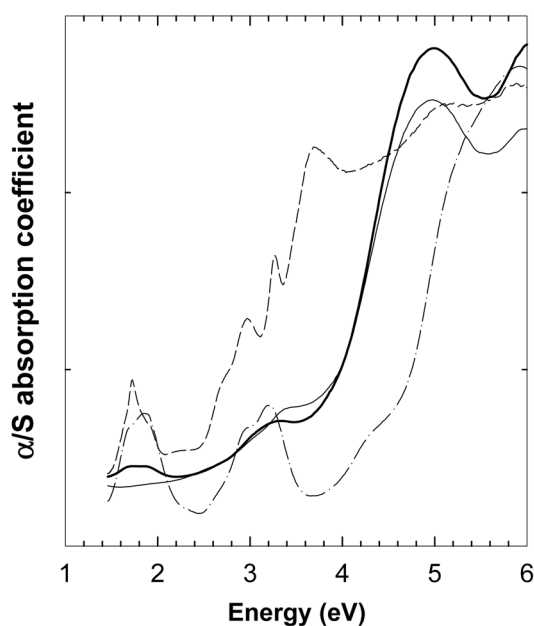


Figure 6. Diffuse reflectance UV-vis absorption spectra for the nickel-intercalated montmorillonite (thick solid lines), the pristine Na-montmorillonite (thin solid lines), NiO (dashed lines), and Ni(OH)₂ (dot-dashed lines).

with those for the pristine montmorillonite clay, nickel oxide, and nickel hydroxide. Like the pristine clay, the intercalate shows an intense absorption peak at 5 eV, corresponding to UV absorption by the host aluminosilicate lattice. In addition, a weak absorption feature corresponding to the d-d transition of divalent nickel ions is observable below 2.0 eV for the intercalation complex like the references NiO and Ni(OH)₂.

Figure 7 displays the FT-IR spectrum of the nickel-

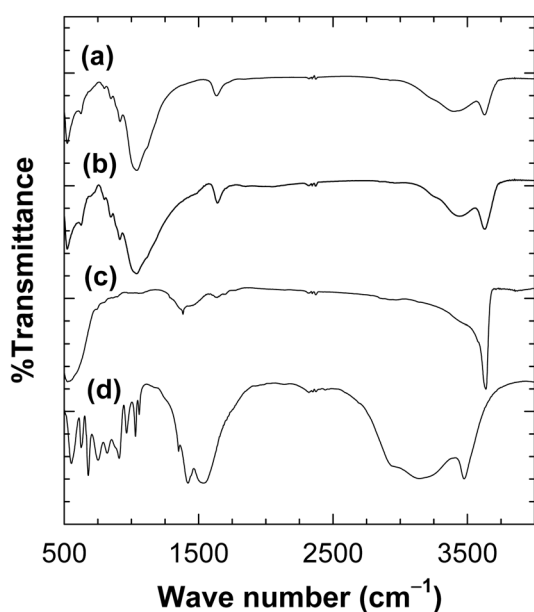


Figure 7. FT-IR spectra of (a) the nickel-intercalated montmorillonite, (b) the pristine Na-montmorillonite, (c) Ni(OH)₂, and (d) Ni(CH₃COO)₂.

intercalated montmorillonite, in comparison with those of the pristine montmorillonite clay, nickel hydroxide, and nickel acetate. Overall spectral features of the intercalate are quite similar to those of the pristine clay; both the materials show characteristic IR bands of O-H stretching and H₂O/H₃O⁺ bending modes at around 3400-3600 and 1630 cm⁻¹, respectively. In contrast to the reference nickel acetate, the intercalate does not show any IR bands corresponding to acetate group in the wave number region of 1300-1600 cm⁻¹, clarifying that the intercalated nickel species are not in the form of nickel acetate.

Ni K-edge X-ray absorption near-edge structure (XANES) spectra for the nickel-intercalated montmorillonite and its calcined derivative are plotted in Figure 8, together with those for the references Ni^{II}(OH)₂, Ni^{II}O, and Ni^{II}(CH₃COO)₂. The edge positions of the intercalation compounds are similar to those of the present references, indicating the divalent state of nickel in these compounds. As shown in Figure 8, all of the present compounds including the Ni-intercalates display only a weak pre-edge peak P corresponding to the quadrupole-allowed 1s → 3d transition.¹⁷ The weak intensity of this feature provides strong evidence on the stabilization of nickel ions in octahedral symmetry.¹⁷ In the main-edge region, the references NiO and Ni(OH)₂ exhibit some fine structures A and B in the middle of edge jump whereas these features are absent in the intercalates. This finding strongly suggests that the intercalated nickel species are stabilized as isolated molecular species, rather than the extended lattice of nickel hydroxide or nickel oxide. Despite the dehydration of guest species upon the calcination, no prominent spectral changes can be observed before and after the heat-treatment, reflecting the maintenance of octahedral symmetry around nickel ions.

We have determined quantitatively the local structure of

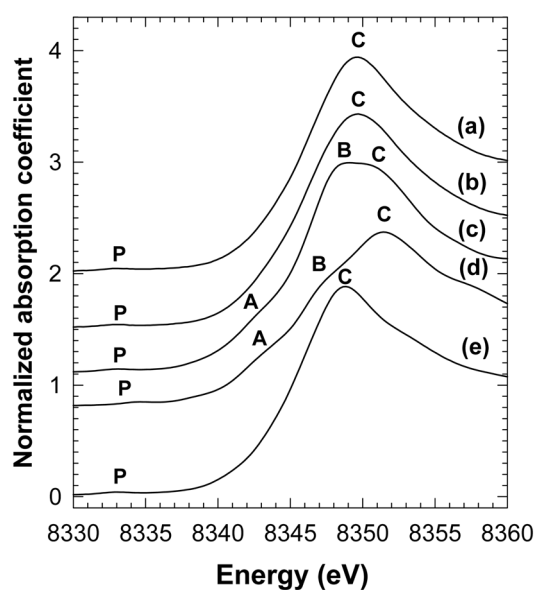


Figure 8. Ni K-edge XANES spectra for (a) the nickel-intercalated montmorillonite and (b) its derivative calcined at 200 °C, in comparison with those for the references (c) Ni(OH)₂, (d) NiO, and (e) Ni(CH₃COO)₂.

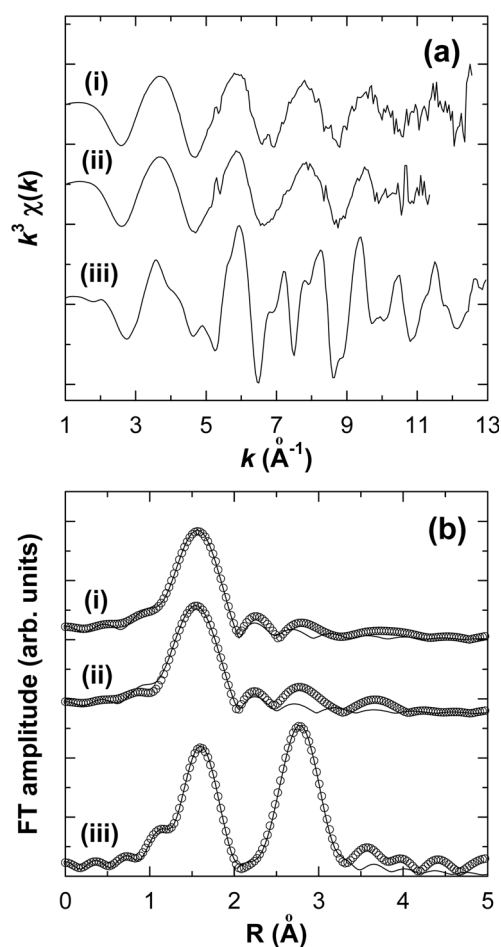


Figure 9. (a) k^3 -weighted Ni K-edge EXAFS oscillations and (b) the Fourier-transformed spectra for (i) the as-prepared nickel-intercalated montmorillonite, (ii) its derivative calcined at 200 °C, and (iii) Ni(OH)₂. The open circles and the solid lines represent the experimental data and the calculated ones, respectively.

intercalated nickel species by performing EXAFS analysis. The k^3 -weighted Ni K-edge EXAFS spectra for the intercalation compound of nickel-montmorillonite, its calcined derivative at 200 °C, and the reference Ni(OH)₂ are plotted in Figure 9a. The experimental EXAFS spectrum of the as-prepared intercalate is quite different from that of the reference Ni(OH)₂, suggesting dissimilar local symmetry around nickel ions in these materials. Between the as-prepared and calcined intercalates, there is only a negligible difference in EXAFS oscillation, indicating little variation of local structure of nickel ions upon the heat-treatment. In the Fourier Transform (FT) diagrams of Figure 9b, the reference Ni(OH)₂ exhibits two intense FT peaks in the R range of 1.0–3.5 Å. While the first peak at ~ 1.6 Å (phase-shift uncorrected) originates from the (Ni–O) coordination shells, the more distant feature at ~ 2.8 Å (phase-shift uncorrected) is related to (Ni–Ni) bonding pairs in edge-shared NiO₆ octahedra. The experimental spectrum of the reference Ni(OH)₂ was quite reproducible with layered CdI₂ structure and the obtained structural parameters are summarized in Table 1. In contrast to the reference Ni(OH)₂, both the as-prepared intercalate

Table 1. Results of non-linear least squares curve fittings for the Ni K-edge EXAFS spectra of the nickel-intercalated montmorillonite, its calcined derivative, and the reference Ni(OH)₂

Sample	bond	CN	R (Å)	σ^2 ($10^{-3} \times \text{\AA}^2$)
Nickel-intercalate-RT ^a	(Ni–O)	6.0	2.05	6.48
Nickel-intercalate-200 °C ^b	(Ni–O)	6.0	2.04	6.74
reference Ni(OH) ₂ ^c	(Ni–O)	6	2.06	6.37
	(Ni–Ni)	6	3.13	6.57

^aThe curve fitting analysis was performed for the range of $1.227 - R - 1.994$ Å and $3.05 - k - 10.90$ Å⁻¹. ^bThe curve fitting analysis was performed for the range of $1.227 - R - 1.994$ Å and $3.1 - k - 9.85$ Å⁻¹. ^cThe curve fitting analysis was performed for the range of $1.166 - R - 3.283$ Å and $3.15 - k - 11.75$ Å⁻¹.

and its calcined derivative display only a single FT peak corresponding to the (Ni–O) shell at around 1.6 Å (phase-shift uncorrected). In this regard, the absence of prominent (Ni–Ni) peak in the FT data of these compounds suggests strongly that the intercalated nickel species exist in the form of isolated molecular form rather than highly linked 2D network like nickel hydroxide, before and after post-calcination. As shown in Figures 9b and 10, the experimental spectra of the intercalates could be well reproduced on the basis of isolated NiO₆ octahedra. As listed in Table 1, regardless of the heat-treatment, the nickel ions are stabilized in the NiO₆ octahedra with (Ni–O) bond distance of 2.05 Å, which are compatible to the (Ni^{II}–O) bond length in the reference Ni(OH)₂ (2.06 Å). Taking into account the absence of (Ni–Ni) shell, we were able to conclude that the nickel species in the as-prepared intercalate exists as an isolated NiO₆ octahedral unit consisting of hydroxyl groups of the host lattice and/or interlayer water molecules. In this context, the present nickel-montmorillonite intercalate is clearly distinguishable from the previously reported 2D

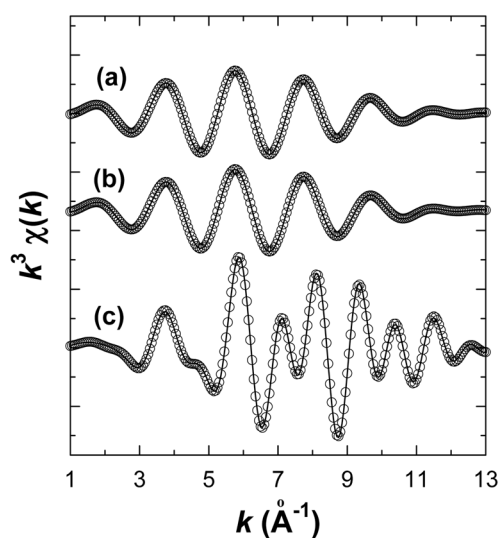


Figure 10. Fourier-filtered Ni K-edge EXAFS data for (a) the as-prepared nickel-intercalated montmorillonite, (b) its derivative calcined at 200 °C, and (c) Ni(OH)₂. The open circles and the solid lines represent the experimental data and the calculated ones, respectively.

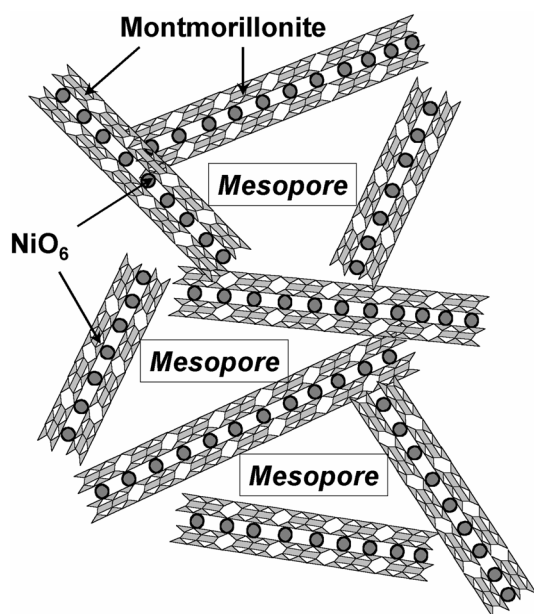


Figure 11. Schematic illustration of the nickel-intercalated montmorillonite.

heterostructured nickel hydroxide-clay compound.¹³ Taking into account the fact that the calcination process gives rise to the evaporation of interlayer water molecules coordinating to nickel ions, the maintenance of the NiO₆ octahedral symmetry in the calcined derivative suggests strongly the formation of stronger covalent bonds between nickel ions and hydroxyl groups of the host lattice.

Based on the experimental findings presented here, we were able to suggest a structural model for the Ni-intercalated aluminosilicate, as illustrated in Figure 11. In this material, the house-of-card stacking of exfoliated clay crystallites forms considerable amounts of mesopores. The present results provide strong evidence on the effectiveness of the exfoliation-restacking reaction for synthesizing mesoporous materials.

Conclusion

In this work, we were quite successful in synthesizing nickel-intercalated montmorillonite compound with mesoporosity. The formation of the heterostructured intercalation complex was evidenced on the basis of the powder XRD, FE-SEM, and UV-vis results. According to the XANES-EXAFS analyses, it becomes clear that the guest species is stabilized as an isolated NiO₆ octahedral unit. Nitrogen adsorption-desorption isotherm measurements clarify that the exfoliation-restacking synthesis adopted here leads to the formation of a considerable amount of mesopores due to the

house-of-card-type stacking of exfoliated clay nanosheets. Taking into account the mesoporosity and high Ni content of the Ni-intercalate, we expect this material to be applicable as efficient catalysts or absorbents.

Acknowledgment. This research (paper) was performed for the Hydrogen Energy R&D Center, one of the 21st Century Frontier R&D Program, funded by the Ministry of Science and Technology of Korea. The experiments at Pohang Light Source (PLS) were supported in part by MOST and POSTECH.

References and Notes

- Jones, S. L. *Catal. Today* **1987**, *12*, 209.
- Handbook of Layered Materials*; Auerbach, S. M.; Carrado, K. A.; Dutta, P. K., Eds; Marcel Dekker: New York, 2004.
- Comprehensive Supramolecular Chemistry*; Atwood, J. L.; Macnicol, J. E. D.; Vogtle, F., Eds.; Pergamon: Oxford, 1996; Vol. 7.
- Choy, J. H.; Jung, H.; Han, Y. S.; Yoon, J. B.; Shul, Y. G.; Kim, H. *J. Chem. Mater.* **2002**, *14*, 3823.
- (a) Bornholdt, K.; Corker, J. M.; Evans, J.; Rummey, J. M. *Inorg. Chem.* **1991**, *30*, 2. (b) Drljaca, A.; Anderson, J. R.; Spiccia, L.; Turney, T. W. *Inorg. Chem.* **1992**, *31*, 4894.
- Burch, R.; Warburton, C. I. *Appl. Catal.* **1987**, *33*, 395.
- Bartley, G. J. J.; Burch, E. *Appl. Catal.* **1985**, *19*, 175.
- Sterte, J. P. *Clays Clay Miner.* **1986**, *34*, 658.
- Hur, S. G.; Kim, T. W.; Hwang, S.-J.; Hwang, S. H.; Yang, J. H.; Choy, J.-H. *J. Phys. Chem. B* **2006**, *110*, 1599.
- (a) Powell, D. A.; Fu, G. C. *J. Am. Chem. Soc.* **2004**, *126*, 7788. (b) Speiser, F.; Braunstein, P.; Saussine, L. *Acc. Chem. Res.* **2005**, *38*, 784. (c) Hu, W. K.; Noreus, D. *Chem. Mater.* **2003**, *15*, 974, and the references therein.
- Handbook of Inorganic Electrochromic Materials*; Granqvist, C. G., Ed.; Elsevier: Amsterdam, 1995.
- (a) Chang, J. S.; Ryu, J. O.; Lee, J. M.; Park, S. E.; Hong, D. Y.; Jhung, S. H. *Bull. Kor. Chem. Soc.* **2005**, *26*, 1512. (b) Pae, Y. I.; Bae, M. H.; Park, W. C.; Sohn, J. R. *Bull. Kor. Chem. Soc.* **2004**, *25*, 1881.
- (a) Ohtsuka, K.; Suda, M.; Ono, M. *Bull. Chem. Soc. Jpn.* **1988**, *61*, 815. (b) Ohtsuka, K.; Suda, M.; Tsunoda, M.; Ono, M. *Chem. Mater.* **1990**, *2*, 511.
- (a) Gupta, G. C.; Malik, W. U. *Clays Clay Miner.* **1969**, *17*, 233. (b) Yamanaka, S.; Brindley, G. W. *Clays Clay Miner.* **1978**, *26*, 21.
- Ohtsuka, K.; Hayashi, Y. *Chem. Mater.* **2001**, *13*, 704.
- Yuan, P.; He, H.; Bergaya, F.; Wu, D.; Zhou, Q.; Zhu, J. *Micropor. Mesopor. Mater.* **2006**, *88*, 8.
- (a) Choy, J. H.; Hwang, S. J.; Park, N. G. *J. Am. Chem. Soc.* **1997**, *119*, 1624. (b) Choy, J. H.; Kim, Y. I.; Hwang, S. J. *J. Phys. Chem. B* **1998**, *102*, 9191. (c) Choy, J. H.; Kim, Y. I.; Hwang, S. J.; Huang, P. V. *J. Phys. Chem. B* **2000**, *104*, 7273.
- (a) Sing, K. S. W.; Everett, D. H.; Haul, R. A. W.; Moscou, L.; Pierotti, R. A.; Rouquerol, J.; Siemieniewska, T. *Pure Appl. Chem.* **1985**, *57*, 603. (b) Carrado, K. A.; Csenesits, R.; Thiyagarajan, P.; Seifert, S.; Macha, S. M.; Harwood, J. S. *J. Mater. Chem.* **2002**, *12*, 3228.